ChemComm

COMMUNICATION

View Article Online
View Journal | View Issue

Cite this: *Chem. Commun.*, 2025, **61**, 19044

Received 20th September 2025,
Accepted 21st October 2025

DOI: 10.1039/d5cc05415j

rsc.li/chemcomm

Uneven Co–N–C-coated graphene as a durable support for low-loading Pt oxygen reduction catalyst

Muyu Xu,†[a] Wenhui Ni,†[a] Yichen Wei,[a] Jun Wang,[a] Mingyu Liu,[a] Ruoxuan Zhi,[a] Junying Wang,*[b] Zelin Wu,*[a] Huinian Zhang*[c] and Junzhong Wang*[a]

An uneven Co–N–C layer coated on electrochemically-exfoliated graphene as an active support ($E_{1/2}$ 0.788 V) to stabilize low-amount Pt catalyst was synthesized. The catalyst exhibited superior oxygen reduction activity (0.72 A mg_{Pt}^{-1}) and durability (10 mV loss after 50k cycles) in acid. Graphene reinforced the metal–support interaction, benefitting the conductivity, activity and durability of the catalyst.

The escalating global energy crisis and environmental pollution necessitate the urgent development of sustainable energy conversion technologies.[1–3] Proton-exchange membrane fuel cells (PEMFCs) and metal–air batteries are among the most promising solutions, yet their widespread application is hindered by the sluggish kinetics of the oxygen reduction reaction (ORR) at the cathode.[4,5] While platinum-based catalysts are state-of-the-art for driving the ORR, their high cost, scarcity, and susceptibility to poisoning present significant economic and practical barriers.[6–9] Consequently, intensive research efforts are being focused on developing low-Pt or Pt-free catalysts that maintain high activity and durability.[10,11]

A big challenge for fuel cell catalysts is their instability, owing to metal dissolution, carbon corrosion, and susceptibility to active site poisoning.[12–14] Strategies to mitigate these issues and reduce platinum loading include alloying Pt with transition metals, engineering core–shell structures, and designing advanced carbon supports.[15,16] Among these, graphene-based supports are highly attractive due to the atomic crystalline 2D material, exceptional electrical conductivity, and superior chemical stability.[17] However, the common use of defective reduced graphene oxide often yields suboptimal results, and the synergistic mechanism between graphene and non-precious metal active sites, such as cobalt-nitrogen-carbon (Co–N–C), remains inadequately understood.[18] Furthermore, the typically amorphous and defective nature of metal–organic-framework-derived carbon supports, while rich in active sites, suffers from poor conductivity and stability, making them vulnerable to corrosion by reactive oxygen species generated during ORR.[19]

Herein, we report a strategy to construct a low platinum loading catalyst supported on graphene sandwiched cobalt–nitrogen–carbon hybrid (G/Co–N–C) to address these challenges. This work is guided by the principle of promoting durability of the carbon support and metal-support interaction. A zeolitic imidazolate framework (ZIF-8) was uniformly deposited onto the electrochemically exfoliated graphene flakes and subsequently pyrolyzed to form a composite support consisting of a highly graphitic graphene base coated with a porous Co–N–C layer (Scheme 1). This structure inhibits graphene stacking, provides abundant nitrogen-related sites for platinum anchoring, and enhances the overall graphitization to improve corrosion resistance. Pt nanoparticles were then deposited *via* a hot-solution process, resulting in a hybrid catalyst (G/Co–N–C@Pt) with excellent dispersion.

The resulting catalyst achieves a remarkable half-wave potential ($E_{1/2}$) of 0.876 V and a mass activity of 0.72 A mg_{Pt}^{-1} in acidic media. More importantly, it demonstrates exceptional durability, retaining its performance with only a 10 mV loss in

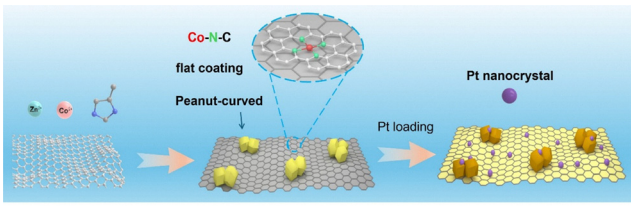

Scheme 1 Synthesis of dispersible active carbon support consisting of graphene and sandwiched Co–N–C uneven layer to support platinum nanocrystals.

[a] *Institutes of Physical Science and Information Technology, Anhui Graphene Carbon Fiber Research Center, Anhui University, Hefei 230601, China. E-mail: 1592577524@qq.com, wangjz@ahu.edu.cn*
[b] *Institute of Coal Chemistry, Chinese Academy of Sciences, Taiyuan 030001, China. E-mail: wangjy@sxicc.ac.cn*
[c] *School of Energy and Power Engineering, North University of China, Taiyuan 030051, China. E-mail: zhanghuinian123@nuc.edu.cn*
† These authors contributed equally to this work.

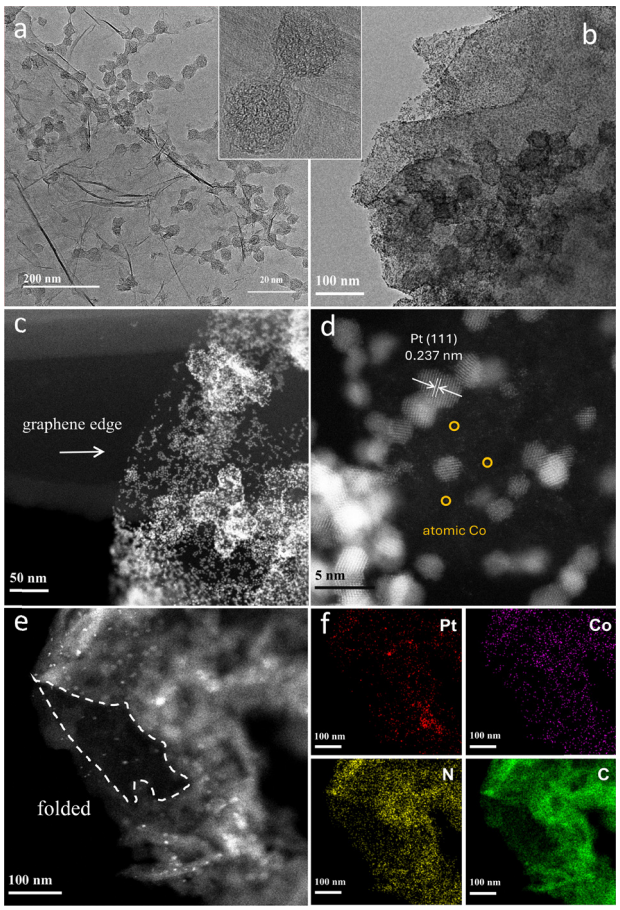

Fig. 1 The morphological structures of (a) carbon support and (b)–(f) catalyst G/Co–N–C@Pt. (a) TEM image of G/Co–N–C, (b) TEM image of G/Co–N–C@Pt, (c) and (d) AC HAADF-STEM images, (e) and (f) EDX analysis of the composition.

halfwave potential ($E_{1/2}$) after 50 000 accelerated stress test cycles. This study elucidates the dual stabilizing role of the interfacial synergistic effect in inhibiting platinum dissolution and maintaining the electrochemical active surface area (ECSA). By correlating support functionalization with the interfacial electronic structure and catalytic durability, we establish a multi-scale design principle for developing high-performance, cost-effective electrocatalysts for next-generation energy devices.

The morphological and structural features of the carbon support G/Co–N–C and the catalyst G/Co–N–C@Pt were characterized by transmission electron microscopy (TEM) and aberration-corrected high-angle annular dark-field scanning transmission electron microscopy (AC HAADF-STEM). As shown in Fig. 1a, the G/Co–N–C carbon support consists of porous, peanut-like nanoparticles (~30 nm) anchored on an ultra-thin Co–N–C layer supported by graphene. This unique sandwiched architecture, featuring interconnected curved islands on a flat coating, provides excellent dispersibility and abundant active sites, facilitating the subsequent uniform deposition of low-loading Pt nanoparticles.

Fig. 1b–f displays the morphology and composition of the G/Co–N–C@Pt catalyst. Pt nanoparticles were uniformly dispersed on the G/Co–N–C support without significant ripening or aggregation. In contrast, control experiments using Co–N–C (without graphene), electrochemically exfoliated graphene, and commercial carbon black under the same synthesis conditions resulted in extensive Pt agglomeration (Fig. S1, SI). The Pt nanocrystals, with average size of 3.2 nm, on the G/Co–N–C are well-dispersed. High-resolution imaging (Fig. 1c) clearly reveals lattice fringes corresponding to the Pt (111) plane with a spacing of 0.237 nm, alongside atomically dispersed Co species. The uneven and porous Co–N–C layer is rich in nitrogen and oxygen functional groups, which serve as anchoring sites for the uniform immobilization of Pt nanocrystals. Energy-dispersive X-ray spectroscopy (EDS) elemental mappings (Fig. 1e and f) confirm the homogeneous distribution of Pt, Co, N, and C throughout the catalyst.

The textural properties of the Co–N–C and G/Co–N–C carbon supports were investigated using N_2 adsorption–desorption isotherms (Fig. S2, SI). Both materials exhibit Type IV isotherms with distinct hysteresis loops, indicative of mesoporous structures. The G/Co–N–C support possesses a slightly lower specific surface area (333.4 $m^2\ g^{-1}$) and a bit larger particle size than the Co–N–C control sample (Table S1, SI). The structural characteristics were further probed by X-ray diffraction (XRD) and Raman spectroscopy. The XRD patterns of G/Co–N–C@Pt, Co–N–C@Pt, and Pt/C (Fig. 2a) show characteristic diffraction peaks at approximately 39.76° and 67.45°, corresponding to the (111) and (220) planes of face-centered cubic (fcc) platinum, respectively.[20] Application of the Debye–Scherrer equation to the Pt (111) peak estimates a crystallite size of 3.2 nm for G/Co–N–C@Pt, slightly smaller than the 3.8 nm calculated for commercial Pt/C.[21] The Co–N–C layer effectively mitigates graphene stacking, facilitating the uniform dispersion of Pt nanocrystals.

Raman spectra (Fig. 2b) of all carbon supports display characteristic D (1340 cm^{-1}, related to defects) and G (1590 cm^{-1}, related to graphitization) bands. The intensity ratio (I_D/I_G) for G/Co–N–C was calculated to be 0.605, which is significantly lower than that of Co–N–C (0.998). This indicates a higher degree of graphitization in the electrochemically exfoliated graphene-composite support, which is beneficial for electrochemical stability.

X-ray photoelectron spectroscopy (XPS) survey scans (Fig. 2c) demonstrate the presence of C 1s, N 1s, O 1s, Co 2p, and Pt 4f on the surface of the G/Co–N–C@Pt catalyst. Deconvolution of the high-resolution N 1s spectrum (Fig. 2d) revealed a higher relative content of graphitic and pyridinic nitrogen in G/Co–N–C@Pt compared to Co–N–C@Pt or G/Co–N–C, suggesting that the incorporation of graphene promotes the formation of these nitrogen species. It is possible that pyrrolic nitrogen serves as the preferred anchoring site for Pt. As seen in the results of inductively coupled plasma (ICP) analysis, G/Co–N–C@Pt loads 11.27 wt% Pt and 1.74 wt% Co, respectively, higher than those for Co–N–C@Pt (7.98 wt% Pt and 0.29 wt% Co) synthesized under same conditions. These results underscore the critical role of the graphene-composite support in enhancing metal uptake and dispersion during catalyst preparation.[22]

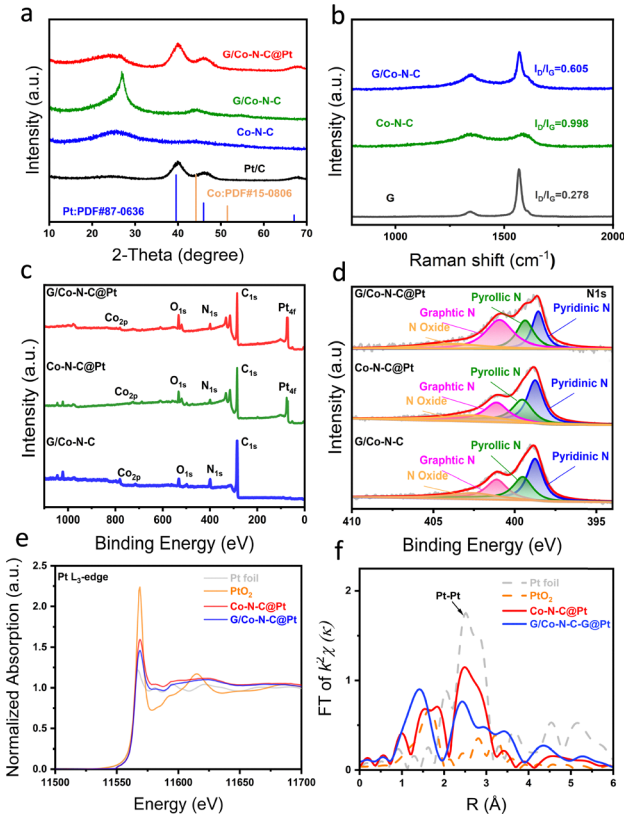

Fig. 2 Spectroscopic analysis of metal-support interaction. (a) XRD patterns, (b) Raman spectra, (c) survey XPS, (d) XPS N element, (e) X-ray absorption near-edge structure (XANES) spectra taken at Pt L3-edge, (f) extended X-ray absorption fine structure (EXAFS) spectra.

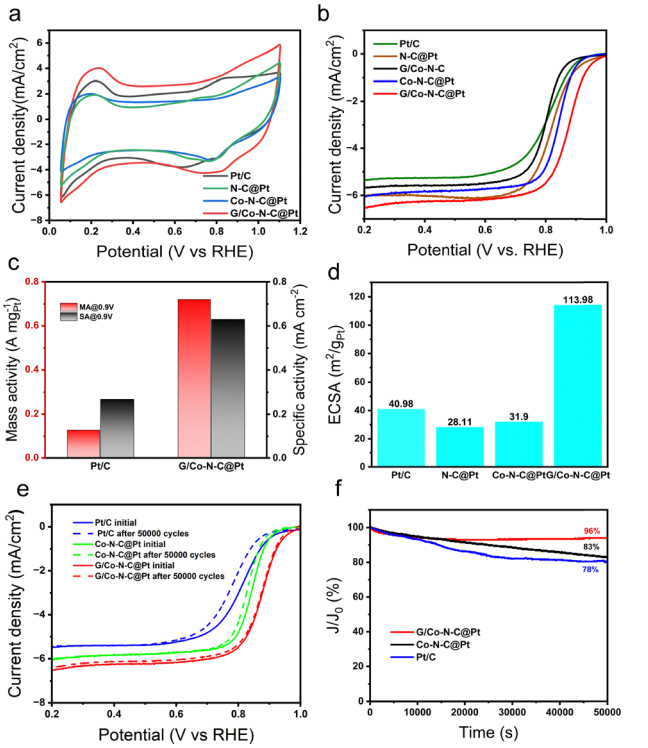

Fig. 3 Electrochemical performance of catalyst G/Co–N–C@Pt compared with control samples. (a) CV curves, (b) LSV curves, (c) mass activity of Pt, (d) ECSA, (e) LSV curves before and after 50 000 cycles, (f) limited current density retention over time (s).

The electronic structure and coordination environment of Pt were probed using X-ray absorption spectroscopy. The XANES spectrum at the Pt L_3 edge (Fig. 2e) displays a positive energy shift along with a reduction in white line intensity for G/Co–N–C@Pt compared to the graphene-free control, suggesting an elevated valence state of Pt and possible electron transfer from Co 3d to Pt 5d orbitals. This modification in electronic structure was further corroborated by the EXAFS spectrum in R-space (Fig. 2f), which shows a dominant peak at ~2.48 Å, corresponding to Pt–Pt metallic coordination, confirming the presence of Pt nanoparticles. Additional features in the spectrum are consistent with a multi-valence Pt environment and a shortened Pt–Pt bond distance, supporting the presence of strong metal-support interactions in the graphene-enhanced composite.[23] Together, these results provide compelling evidence for enhanced electronic coupling between Pt and the Co–N–C support, which contributes to improved catalytic properties.

The electrochemical performance of G/Co–N–C in acidic condition (0.1 M $HClO_4$) was tested. Linear sweep voltammetry (LSV) was performed on G/Co–N–C at rotation speeds ranging from 400 to 2025 rpm to investigate the ORR pathway in acidic medium. The average electron transfer number (n) calculated from the Koutecký–Levich plots (Fig. S3, SI) was 3.91, indicating that the ORR proceeds primarily *via* a highly efficient four-electron pathway. G/Co–N–C presents a stable half-wave potential ($E_{1/2}$ 0.788 V) and a loss of only 16 mV after 20 000 cycles (Fig. S4, SI). Fig. S5 (SI) shows the higher stability of G/Co–N–C than the Co–N–C sample and good methanol tolerance. The incorporation of graphene promotes catalytic stability.

Fig. 3a presents the cyclic voltammetry (CV) curves recorded in O_2-saturated 0.1 M $HClO_4$. The G/Co–N–C@Pt catalyst exhibits a Pt electrochemical oxidation peak consistent with that of commercial Pt/C. The voltammetric features can be assigned as follows: the region between 0.05–0.4 V corresponds to hydrogen underpotential adsorption/desorption, 0.4–0.8 V to the electric double-layer region, and 0.8–1.1 V to Pt oxidation and reduction. Linear sweep voltammetry (LSV) measurements reveal that G/Co–N–C@Pt delivers the best oxygen reduction reaction (ORR) performance among the Pt-based catalysts studied. As shown in Fig. 3b and Fig. S6 (SI), in 0.1 M $HClO_4$, it achieves the highest half-wave potential (0.88 V), onset potential (0.99 V), mass activity (0.72 A mg^{-1}), and specific activity (0.62 mA cm^{-2}). Furthermore, Fig. 3c and d demonstrate that its mass activity at 0.90 V is six times greater than that of commercial Pt/C, along with a high electrochemical active surface area (ECSA = 113.98 m^2 g^{-1}). The Tafel slope of G/Co–N–C@Pt (27.34 mV dec^{-1}, Fig. S7, SI) is lower than those of the other catalysts, indicating superior ORR kinetics. Additionally, electrochemical impedance spectroscopy (Fig. S8, SI) reveals the smallest semicircle diameter for G/Co–N–C@Pt, reflecting the lowest charge transfer resistance, which should result from the superior conductivity of graphene.

As shown in Fig. 3e, the half-wave potentials of commercial Pt/C, Pt/G, Pt/Co–N–C, and Pt/Co–N–C-G catalysts exhibited varying degrees of decline with an increasing number of electrochemical accelerated cycles. Pt/Co–N–C–G demonstrated superior ORR stability to commercial Pt/C for the control sample without graphene, maintaining its performance well before and after cycling in terms of ECSA, mass activity, and specific activity (Table S2, SI). G/Co–N–C@Pt exhibited the highest stability among all catalysts after repeated potential cycling. Chronoamperometric testing at 0.65 V (*vs.* Ag/AgCl) further demonstrated exceptional long-term stability, with G/Co–N–C@Pt retaining 96% of its initial current density after 50 000 seconds (Fig. 3f). Post-test characterization *via* XRD and XPS revealed minimal structural changes, confirming the robust stability of the catalyst (Fig. S9 and S10, SI). Moreover, the average particle size of G/Co–N–C@Pt increased only marginally from 3.2 nm to 3.5 nm while maintaining uniform dispersion, with significantly less agglomeration than observed in Pt/C, which increased from 3.8 nm to 4.5 nm (Fig. S11 and S12, SI). These results collectively demonstrate that the superior electrochemical durability of G/Co–N–C@Pt over commercial Pt/C and other control samples originates from its enhanced structural stability.

In summary, we have successfully designed and synthesized a low-platinum catalyst (G/Co–N–C@Pt) by depositing Pt nanocrystals onto a graphene-sandwiched cobalt-nitrogen-carbon composite support *via* solution method. The support features a unique peanut-island attached ultra-thin layer of Co–N–C coated on graphene, offering high conductivity and excellent electrochemical performance. It demonstrates good durability in acidic media, with the half-wave potential shifting only from 0.788 V to 0.772 V, thereby compensating for the catalytic losses typically associated with reduced Pt loading. The G/Co–N–C@Pt (10 wt% Pt) catalyst exhibits outstanding ORR performance, including a high half-wave potential (0.88 V), superior mass activity (0.72 A mg^{-1}), and exceptional stability (only 10 mV loss after 50 000 cycles). This enhanced activity and durability originate from synergistic metal–support interactions, facilitated by graphene-induced graphitic/pyridinic N-sites and Co–N_x moieties, which stabilize Pt nanoparticles and decrease dependence on platinum. This work provides a promising strategy for developing cost-effective electrocatalysts for fuel cell and metal-air battery applications.

We acknowledge the financial support by grants from National Natural Science Foundation of China (22279001, 22179138).

Conflicts of interest

There are no conflicts to declare.

Data availability

The data supporting this article have been included as part of the supplementary information (SI). Supplementary information is available. See DOI: https://doi.org/10.1039/d5cc05415j.

Notes and references

1 D. Dang, L. Zhang, G. Long, C. Liu, W. Fan, J. Zheng, T. Wang, Q. Liu and X. Han, *Appl. Catal., B*, 2025, **379**, 125679.
2 J. Jewell, D. McCollum, J. Emmerling, C. Bertram, D. E. H. J. Gernaat, V. Krey, L. Paroussos, L. Berger, K. Fragkiadakis, I. Keppo, N. Saadi, M. Tavoni, D. van Vuuren, V. Vinichenko and K. Riahi, *Nature*, 2018, **554**, 229–233.
3 K. Jiao, J. Xuan, Q. Du, Z. Bao, B. Xie, B. Wang, Y. Zhao, L. Fan, H. Wang, Z. Hou, S. Huo, N. P. Brandon, Y. Yin and M. D. Guiver, *Nature*, 2021, **595**, 361–369.
4 N. Liu, Y. Li, W. Liu, Z. Liang, B. Liao, F. Yang, M. Zhao, B. Yan, X. Gui, H. B. Yang, D. Yu, Z. Zeng and G. Yang, *Nano-Micro Lett.*, 2025, **17**, 203.
5 M. I. Maulana, T. H. Jo, H.-Y. Lee, C. Lee, C. Gyan-Barimah, C.-H. Shin, J.-H. Yu, K.-S. Lee, S. Back and J.-S. Yu, *J. Am. Chem. Soc.*, 2024, **146**, 30922–30932.
6 K. Kodama, T. Nagai, A. Kuwaki, R. Jinnouchi and Y. Morimoto, *Nat. Nanotechnol.*, 2021, **16**, 140–147.
7 X. Liu, Y. Wang, J. Liang, S. Li, S. Zhang, D. Su, Z. Cai, Y. Huang, L. Elbaz and Q. Li, *J. Am. Chem. Soc.*, 2024, **146**, 2033–2042.
8 Z. Zhao, C. Chen, Z. Liu, J. Huang, M. Wu, H. Liu, Y. Li and Y. Huang, *Adv. Mater.*, 2019, **31**, 1808115.
9 H. Wu, J. Lv, H. Peng, P. Cai, H. Zhang, F. Xu and L. Sun, *Int. J. Hydrogen Energy*, 2024, **70**, 195–199.
10 A. Ali, A. Laaksonen, G. Huang, S. Hussain, S. Luo, W. Chen, P. K. Shen, J. Zhu and X. Ji, *Nano Res.*, 2023, **17**, 3516–3532.
11 R. Bai, Q. Ye, C. Li, H. Wang, Y. Zhao, Y. Zhang, Y. Zhou and X. Zhao, *Adv. Sci.*, 2025, **12**, 2502002.
12 T. Gan, L. Tao, Z. Zhang, A. Zhou, Y. Chen, J. Li, S. Zhang, S. Du and Y. Li, *J. Am. Chem. Soc.*, 2025, **147**, 32729–32736.
13 H. Li, J. You, X. Cheng, L. Luo, X. Yan, J. Yin, S. Shen and J. Zhang, *ACS App. Mater. Interfaces*, 2023, **16**, 540–554.
14 M. Tang, H. Yan, X. Zhang, Z. Zheng and S. Chen, *Adv. Mater.*, 2023, **37**, 2306387.
15 Y. D. Wang, Q. Meyer, K. Tang, J. E. McClure, R. T. White, S. T. Kelly, M. M. Crawford, F. Iacoviello, D. J. L. Brett, P. R. Shearing, P. Mostaghimi, C. Zhao and R. T. Armstrong, *Nat. Commun.*, 2023, **14**, 745.
16 H. Khani, N. S. Grundish, D. O. Wipf and J. B. Goodenough, *Adv. Energy Mater.*, 2019, **10**, 1903215.
17 H. Zhang, J. Wang, Z. Zhao, H. Zhao, M. Cheng, A. Li, C. Wang, J. Wang and J. Wang, *Green Chem.*, 2018, **20**, 3521–3529.
18 M. Wang, K. Sun, W. Mi, C. Feng, Z. Guan, Y. Liu and Y. Pan, *ACS Catal.*, 2022, **12**, 10771–10780.
19 G. Cai, W. Zhang, L. Jiao, S.-H. Yu and H.-L. Jiang, *Chem*, 2017, **2**, 791–802.
20 Y. Xiong, Y. Ma, L. Zou, S. Han, H. Chen, S. Wang, M. Gu, Y. Shen, L. Zhang, Z. Xia, J. Li and H. Yang, *J. Catal.*, 2020, **382**, 247–255.
21 N. Jahan Tamanna, M. Sahadat Hossain, N. Mohammed Bahadur and S. Ahmed, *Results Chem.*, 2024, **7**, 101313.
22 Y. Zhou, J. Chen, Z. Huang, Y. Peng, L. Xing, C. Tang, N. Wang, L. Meng, M. Wu, L. Du and S. Ye, *Nanoscale*, 2024, **16**, 5215–5221.
23 L. Zhao, Z. Zhu, J. Wang, J. Zuo, H. Chen, X. Qi, X. Niu, D. J. Blackwood, J. S. Chen and R. Wu, *Adv. Mater.*, 2025, **37**, 2502457.